MARINE MAMMAL SCIENCE, 30(2): 726–746 (April 2014)

DOI: 10.1111/mms.12083

Drag of suction cup tags on swimming animals: Modeling and measurement

K. Alex Shorter,[1] Department of Mechanical Engineering, University of Michigan, 2350 Hayward Street, Ann Arbor, Michigan 48109, U.S.A.; **Mark M. Murray**, Mechanical Engineering Department, United States Naval Academy, 590 Holloway Road, Annapolis, Maryland 21402, U.S.A.; **Mark Johnson**, Scottish Oceans Institute, University of St Andrews, St Andrews, Fife KY16 8LB, United Kingdom and Department of Bioscience, University of Aarhus, DK-8000 Aarhus C, Denmark; **Michael Moore**, Biology Department, Woods Hole Oceanographic Institution, Woods Hole, Massachusetts 02543, U.S.A.; **Laurens E. Howle**, Pratt School of Engineering, Duke University, Durham, North Carolina 27708, U.S.A. and BelleQuant Engineering, PLLC, 7813 Dairy Ridge Road, Mebane, North Carolina 27302-9281, U.S.A.

Abstract

Bio-logging tags are widely used to study the behavior and movements of marine mammals with the tacit assumption of little impact to the animal. However, tags on fast-swimming animals generate substantial hydrodynamic forces potentially affecting behavior and energetics adversely, or promoting early removal of the tag. In this work, hydrodynamic loading of three novel tag housing designs are compared over a range of swimming speeds using computational fluid dynamics (CFD). Results from CFD simulation were verified using tag models in a water flume with close agreement. Drag forces were reduced by minimizing geometric disruptions to the flow around the housing, while lift forces were reduced by minimizing the frontal cross-sectional area of the housing and holding the tag close to the attachment surface. Hydrodynamic tag design resulted in an experimentally measured 60% drag force reduction in 5.6 m/s flow. For all housing designs, off-axis flow increased the magnitude of the force on the tag. Experimental work with a common dolphin (*Delphinus delphis*) cadaver indicates that the suction cups used to attach the types of tags described here provide sufficient attachment force to resist failure to predicted forces at swimming speeds of up to 10 m/s.

Key words: bio-logging, CFD, hydrodynamic tag design, suction cups.

As sensing and electronics technology improve, bio-logging tags are enabling the collection of increasingly sophisticated behavioral information from free ranging

[1]Corresponding author (e-mail: kshorter@whoi.edu).

marine animals in their natural environment (Madsen *et al*. 2002, Johnson and Tyack 2003, Cooke *et al.* 2004, Ropert-Coudert *et al.* 2007). Bio-logging tags are integrated mechanical and electrical systems containing sensors, data sampling electronics, a protective housing, and a means of attachment to the animal. Tags that telemeter data also require an antenna directed away from the body of the animal to radiate effectively. Conversely, archival tags that record data for later retrieval must have floatation to enable recovery once the tag detaches from the animal. Each of these components introduces constraints that drive the tag design. For example, accelerometry sensors used to measure animal movement require attachment methods that fix the orientation of the sensor with respect to the animal (van Dam *et al.* 2002, Miller *et al.* 2004, Viviant *et al.* 2010). This restricts the use of reorientation schemes that align the tag with the flow and so reduce drag (Aoki *et al.* 2007).

For cetaceans, suction cups are a widely used method to attach short-duration archival tags (Hooker and Baird 2001), but longer-term tags are also attached with bolts through the dorsal fin (Read and Westgate 1997) or barbs implanted in the epidermis, blubber, or muscle (Mate *et al.* 2007, Andrews *et al.* 2008). The most appropriate attachment method depends on the longevity of the tag and the behavior of the target species. Archival tags that sample high-rate sensors such as wide bandwidth accelerometers, hydrophones, or cameras typically use a short-term, minimally invasive attachment, such as suction cups, that is compatible with the limited recording capacity of the tag and the need to recover the device to obtain the data. For longer-term devices, a more reliable, skin-penetrating attachment is preferred. However, no matter the attachment method, the presence of a tag increases the net loading on the animal as it moves through the water and can impact its behavior, maneuverability, and energetics (Ropert-Coudert and Wilson 2005).

The hydrodynamic loading of tags is particularly relevant for the many marine animals with highly streamlined bodies for which a small disturbance in flow may cause a disproportionate increase in the cost of transport (Fish 1998). While the relative impact of the tag will depend on both the size of the tag and animal, this impact will be most pronounced for long attachments and on animals that move large distances, *e.g.*, on seasonal migrations or foraging trips, because the parasitic drag increasingly becomes an energy budget issue for the animal (Wilson *et al.* 1986, Wilson and McMahon 2006). For example, Wilson and McMahon (2006) demonstrated that a 200 mm long × 3 mm diameter antenna resulted in up to 5× reduction in foraging efficiency of tagged Magellanic penguins (*Spheniscus magellanicus*; Wilson *et al.* 2004). However, there are relatively few studies of the impact of tags on marine animals, due in part to the fundamental difficulty of quantifying the performance of control (*i.e.,* untagged) animals with the same resolution as tagged animals. Even though tags may affect animals in ways other than hydrodynamic loading, the work of Wilson *et al.* (2004) suggests that one proxy for tag impact is increased cost of movement caused by the tag. Thus, the relative impact of different tag designs can be assessed by estimating the additional force that must be produced by the animal to swim at a given speed (Hanson 2001, Pavlov *et al.* 2007).

The swim speed of the animal is a major factor determining the additional force resulting from a tag. Forces from flow disturbance tend to increase as velocity-squared making high swimming speeds of paramount concern (Munson *et al.* 2006). Maximum swim speeds for cetaceans typically occur during brief events such as foraging chases or predator escape that last on the order of seconds and vary a great deal between species. For mysticetes these speeds can be as high as 13 m/s and odontocetes have been observed at speeds of 15 m/s (Fish and Rohr 1999, Sato *et al.* 2007,

Watanabe *et al.* 2011). Short-finned pilot whales (*Globicephala macrorhynchus)* have been recorded swimming at up to 9 m/s during foraging chases (Aguilar Soto *et al.* 2008). However, sustained speeds, defined by Fish and Rohr (1999), as activity lasting at least 15 s, are much lower for all cetaceans. Peak sustained swim speeds are estimated at 5 m/s for mysticetes and 7 m/s for odontocetes (Fish and Rohr 1999). Thus, the impact of a tag may vary with the behavior of the animal and its reliance on fast swimming, both of which may be unknown prior to tagging. A number of additional factors also impact the forces resulting from a tag attachment: body motion during active swimming; the attachment location and orientation of the tag, which depend on the position of the animal at the tagging moment; the height of the tag above the skin surface; and the uncertain and dynamic character of the fluid boundary layer around the animal (Fish and Rohr 1999).

Given the complexities of the flow field around a tag on an animal, computational fluid dynamics (CFD) methods offer an efficient way to assess the performance of different designs before they are built and deployed. These methods involve estimating the flow around a simulated shape by dividing the test volume into small elements and solving the differential equations governing flow for each element. Pavlov *et al.* (2007) utilized CFD to create a dolphin dorsal fin tag design that reduced the forces on the animal created by the tag. The authors used parametric models of the dorsal fin to evaluate the hydrodynamic performance of two alternative tag configurations under a range of flow velocities. The study provided a general methodology for applying computer aided design (CAD) and CFD to tag design. More recently, the same authors applied this modeling approach to design a noninvasive dolphin dorsal fin tag in which lift forces acting on the tag are used passively to secure the tag to the fin (Pavlov and Rashad 2011). However, the studies of Pavlov *et al*. (2007) and Pavlov and Rashad (2011) have yet to be validated experimentally, a critical step to establish confidence in the predictive performance of CFD (Weber *et al.* 2011).

In this work, we use a combination of CFD and experimental testing to explore novel suction cup tag designs for large whales. The tags described here are custom engineered and are intended to make accurate orientation measurements and so use a rigid multi-cup attachment to the animal. To simplify the CFD problem, we examine the forces created by steady fluid flow around tags secured to a flat rigid surface. These assumptions neglect additional forces and flow that result from body motion and skin flexure, but are reasonable because this is a comparative design study where each tag will be evaluated under the same conditions. The contributions of this paper are three fold. First, this work provides insight into hydrodynamic housing design and the resulting forces created by bio-logging tags on large whales. Second, these results illustrate how a virtual testing environment both accelerates the design process and provides information that is not available from on-animal testing alone. Finally, the simulation results are validated experimentally, demonstrating that the assumptions inherent in the simulation are acceptable.

Methods

Forces Acting on the Tag

As a tag attached to an animal moves through the water it experiences a net force due to the fluid flow around it. The force component acting parallel to the flow is called drag, the component acting perpendicular to the attachment surface is lift, and

the component normal to the flow and parallel to the attachment surface is the side force (Munson *et al.* 2006). The net force acting on the tag will also generate moments that are dependent on the geometry of the tag, the location of the attachment to the animal, and the magnitude and direction of the forcing from the fluid. These additional forces were not explicitly modeled but are most likely small in comparison to the linear forces given the small body size of the tag. Viscous shear and pressure forces contribute to the net force on the tag. These forces are caused by the change in momentum of the fluid as it moves past the tag and are a function of the shape and surface finish of the tag (Munson *et al.* 2006). Additional pressure differentials in the fluid surrounding the tag arise when the flow becomes separated from the surface of the tag and creates low-pressure regions downstream called a wake. The forces acting on the tag are further complicated by the proximity of the large flexible surface of the whale that creates its own flow regime as the animal moves through the water.

Tag Designs

The tag housing designs considered here are for a noninvasive acoustic archival tag intended for 1–2 d deployments on free-swimming animals. The design constraints include: a rigid housing for mounting and protection of the electronics, a multi-point attachment to the animal, adequate flotation, two forward-facing hydrophones, and a rear-facing VHF antenna. After releasing from the animal, the tag must float at the surface with the antenna out of the water requiring a center of buoyancy (CB) that is posterior of the center of gravity (CG). This is achieved by placing the floatation behind the electronics and battery. Because the tag will be deployed on unrestrained animals, *e.g.*, with a pole, there is little control over the orientation or location of the tag on the animal. The tags described in this work use four suction cups to fix the orientation on the animal, but forces acting on the tag from the fluid flow or contact from other animals can reorient the tag during an attachment. In each design, the tag electronics are packaged in a hard plastic box for protection (Fig. 1). A block of syntactic foam sits behind the tag electronics to provide floatation. The electronics, hydrophones, and foam assembly are molded into a urethane shell to define the external shape. Four 45 mm diameter silicone cups are used to make a rigid attachment to the animal. We consider two alternative designs within these constraints.

Model A, was designed to have minimum surface area in all attachment orientations for a given internal volume and CG-CB separation (Fig. 1, Table 1). This leads to a box-shaped envelope that diverges from the smooth tapering shapes normally used to minimize hydrodynamic forces. Attachment points for the suction cups add to the complexity of the external form and create potential points of flow disturbance.

Model B attempts a compromise between surface area and hydrodynamic form leading to a larger but smoother-bodied tag (Fig. 1, Table 1). This streamlined half-body screens the cups and minimizes the geometric disruptions to the flow. The design also includes a channel under the tag to reduce the lift component of the force acting on the tag. The channel is intended to increase the flow speed under the tag to match the increased flow velocity over the top of the housing and so reduce the pressure differential across the tag.

For both tag designs, the proximity of the animal's skin surface with its attendant boundary layer and complex flow make it difficult to predict how water will flow around the tag. To assess the impact of attachment height on tag performance, we produced a third design (Model C) in which the tag is housed in a conventional tear-

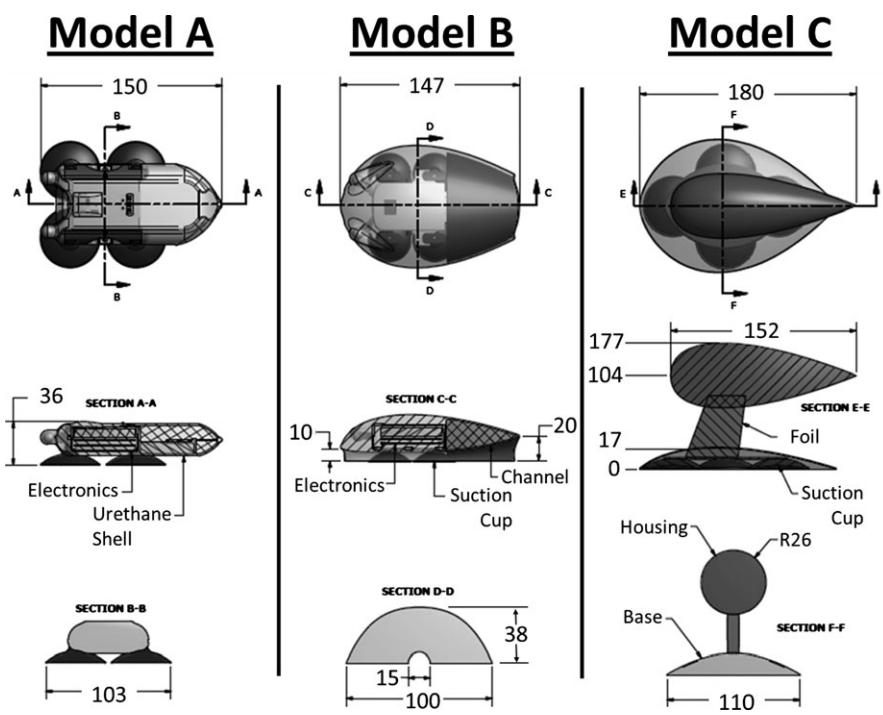

Figure 1. Tag housing designs in plan view (upper panels), longitudinal cross-section (middle panels) and frontal cross-section (bottom panels). The longitudinal cross-sections are taken along the center line of the tags (marked A-A in the upper panels). The frontal cross-section is the outer envelope of the shape that is exposed to the flow when the tag is aligned with its longitudinal axis parallel to the direction of motion (marked B-B in the upper panels). Dimensions are in millimeters.

Table 1. Maximum dimensions, frontal areas, and volumes for the three tag designs.

Tag design	Maximum length (mm)	Maximum width (mm)	Maximum height (mm)	Volume (mm^3)	Maximum frontal cross-sectional area (mm^2)
Model A	150	103	36	245×10^3	2,200
Model B	147	100	38	188×10^3	2,700
Model C	180	110	177	322×103	3,800
Model C, no base	152	53	53	184×10^3	2,200

drop form mounted well away from the boundary layer associated with flow around the animal (Model C; Fig. 1, Table 1). A hydrodynamic foil attaches the tag body to a streamlined base that houses the suction cups. This design is impractical for a number of reasons. The high profile of the tag exposes it to fouling and contact with other animals. The increased hydrodynamic moment of the design increases loading on the suction cups, and the thin strut reduces the stability of the platform increasing noise in the accelerometer measurements. Nonetheless, this model provides an opportunity to assess the drag contribution of the tag shape without the additional

complexity of flow over the skin surface. The model was used in CFD simulations but no flume trials were attempted with this shape.

Autodesk Inventor 11 (Autodesk, Inc., San Rafael, CA) was used to create solid models of the tags for computational analysis and experimental testing. Full-scale models of designs A and B were made from ABS plastic using fused deposition modeling (FDM, Fig. 1). The design A model included the geometry of four compressed suction cups. This rapid prototyping (RP) process has a layer thickness of 0.254 mm and so produces slightly rough surfaces which may add to the surface drag of the shapes. However, a similar RP process is used by the authors to produce molds for fieldable tags making the models realistic.

The thin, flexible VHF antenna normally included in a tag for radio tracking is difficult to simulate because it can be displaced by the flow and was excluded from both the simulated and physical models. Neglecting the antenna was justified because our goal was to conduct a comparative study of tag geometry on flow forces and each tag would use the same antenna. Therefore, forces (primarily drag) added by the antenna would be approximately the same for each tag design at corresponding flow speeds. To provide additional context for this work, the drag loading of the 21 cm (0.5 mm diameter) antenna was examined independently. We expect that the antenna would deflect to 3/4–1/2 of its original length when the tag is oriented broadside (90°) to the oncoming flow at the fastest simulated flow speed (10 m/s). For the flow speeds used in the simulations (0.25–10.0 m/s), the antenna would experience Reynolds numbers in the range of $125 \leq Re \leq 5{,}000$ in the broadside orientation. In this range of Reynolds numbers, the drag coefficient for flow over a cylinder is approximately 1.0–2.0, with the lower Reynolds number generating the greater drag coefficient (Fox and McDonald 1999). The drag added by the antenna would have a magnitude of approximately 0.007 N at the lowest flow speed considered (0.25 m/s) ranging to approximately 2.5 N at the fastest flow speed considered (10.0 m/s). However, these drag estimates represent the worst case of 90° tag orientation. For the 0° orientation, the antenna, which projects rearward and horizontal from the tag, would be in the tag's wake region and would not experience significant drag compared to the drag and lift forces of the tag body. Additionally, the buoyancy force and associated moments that result from the floatation in the rear of the tag were not considered because the force is about 1% of the forces expected from fluid flow.

Computational Fluid Dynamics (CFD) Modeling and Simulations

Computational fluid dynamics analysis was used to compare the performance of the three tag designs. The forces acting on each design were calculated over a range of flow speeds (0.25–10 m/s) and flow orientations (0°–180°) during steady and unsteady flow field simulations. The flow speed was held constant during each trial, a condition more indicative of an animal "gliding" through the water without the additional variable flow generated by swimming motions. For simplicity, the simulation also does not account for modifications to the flow field that would be created by features on the animal's body (*e.g.*, dorsal or pectoral fins). Flow fields around 3D CAD models of the tag were simulated using the SolidWorks 2013 Flow Simulation package (Dassault Systemes SolidWorks Corporation, Waltham, MA). Simulations were performed in a computational domain with dimensions 400 mm wide × 400 mm high × 1,800 mm long (Fig. 2). The width, height, and length of the domain are 2, 2, and 10 times larger than the largest tag design dimension, respectively. The lower surface of the model was placed in the center of the lower boundary wall, with the center of

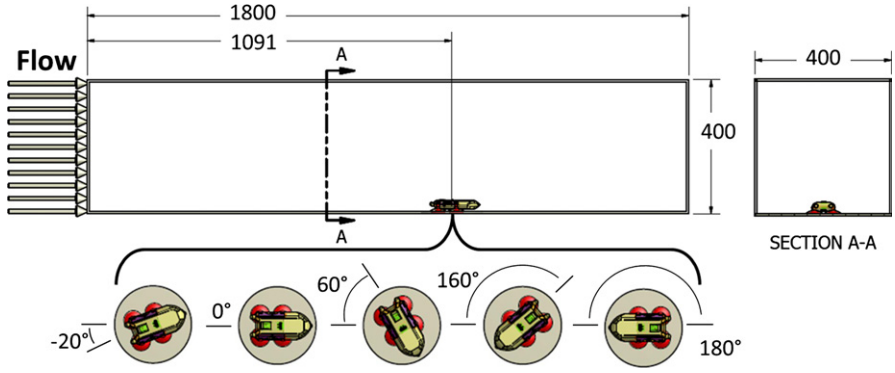

Figure 2. An illustration of the Model A tag in the computational domain used for the simulations of all tag designs. The fluid flow is from left to right and representative orientations of the tag to the flow are shown at the bottom of the figure.

the tag 1,091 mm from the inlet plane. Boundary conditions for the steady Favre-averaged Navier-Stokes (FANS) simulations consisted of real wall (no slip) flow conditions on the lower wall, and ideal wall (free slip) conditions on the side and upper walls. The simulations employed transport equations for turbulent kinetic energy and turbulent energy dissipation rate (model). The default wall roughness and turbulence parameters were used as these gave reasonable results in our previous work (Weber *et al.* 2011). The flow solver used a single system of equations to simulate laminar and turbulent flow with transition between these flow regimes enabled. Laminar to turbulent transition was handled *via* the method of modified wall functions using Van Driest's profile instead of a logarithmic profile. Integral boundary layer theory was used if the local mesh size was smaller than the local boundary layer. Additional details of the simulation methods are available in the SolidWorks Flow Simulation technical documentation (Dassault Systemes SolidWorks Corporation, Waltham, MA). The inlet plane was constrained to uniform flow speed and either a uniform total or static pressure exit boundary condition was used. As inconsistent results were obtained with the automatic mesh refinement feature of the software, we manually specified the mesh geometry to concentrate finite volume cells near the tag CAD models. After performing a mesh convergence study covering the range from 3.3×10^6 to 1.7×10^7 finite volume cells, we selected a mesh with approximately 3.3×10^6 cells for the majority of the simulations. This cell count gave a reasonable combination of convergence accuracy and simulation time. The average solution time on an 32 core PC with 64 GB of RAM was approximately 8 h per simulation.

Experimental Validation of the CFD Models

Water tunnel experiments were conducted at the United States Naval Academy in Annapolis, Maryland (Fig. 3). The water tunnel had a test section of 400 mm square × 1,800 mm long. The tunnel employed turning vanes in the corners and a honeycomb flow straightener in the settling chamber. Free-stream turbulence was ~0.5% (Schultz and Flack 2003). Models were evaluated at five flow speeds ranging from 1 m/s to 5.6 m/s with a constant orientation to the flow (0°), and at 12 orientations ranging from −20° to 90° at constant 5.6 m/s flow (with the zero angle indicating tag alignment with the flow). These flow speeds and orientations were selected to

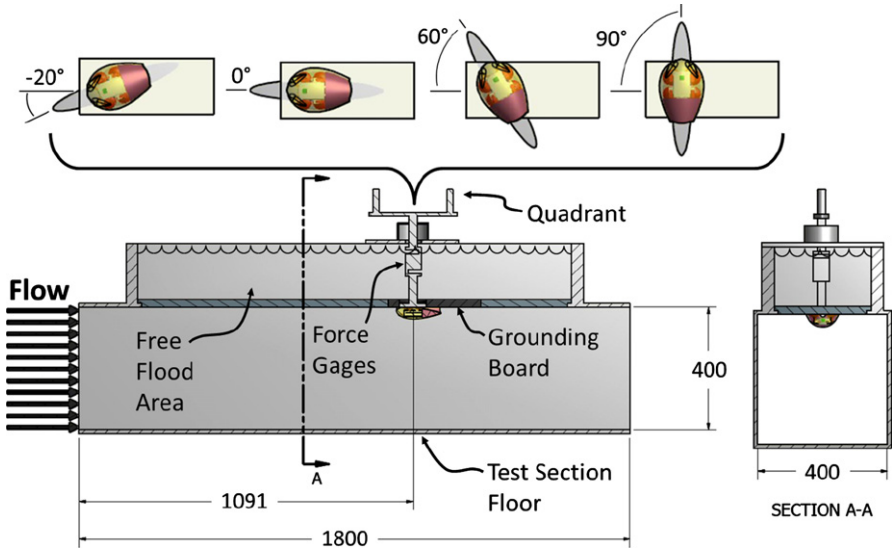

Figure 3. An illustration of the Model B tag in the water tunnel. Both models were mounted to the load cell *via* an extension used to submerge the test piece upside-down below the surface of the water tunnel. A grounding board surrounded the extension where the test piece was mounted to create a uniform ceiling for the test section, but the space above the grounding board was flooded.

span the range of configurations that could be tested in the flow tank. Measurements of lift, drag, and side forces were made with submersible Hydronautics force transducers and the angle of the model was measured by a multi-turn potentiometer mounted on a custom built quadrant (Weber *et al.* 2009). The tag models were mounted to the load cell *via* an extension used to submerge the test piece upside-down below the surface of the water tunnel. Tag models were secured to the extension using mechanical fasteners. A grounding board surrounded the extension where the test piece was mounted to create a uniform ceiling for the test section, and the space above the grounding board was flooded.

Drag coefficients provide a metric for comparing tag designs and were calculated from the simulated and experimental data using the following equation (Munson *et al.* 2006):

$$C_d = \frac{2F_d}{\rho v^2 A}, \tag{1}$$

where v is the mean speed of the fluid (restricted here to 0.25–10 m/s in simulations and 1–5.6 m/s in the water tunnel), ρ is the density of water (1,000 kg/m^3), F_d is the magnitude of the drag from the simulations or water tunnel measurements, and A is the projected frontal area of the tag with respect to the flow direction.

Load Testing of the Model A Tag

The attachment that secures the tag to the animal must be able to resist the forces generated by fluid flow around the tag. For suction cups, the attachment force is

created by the pressure differential between the water outside the cup and the air-filled internal volume formed by the cup and the animal's skin. When the cup is loaded perpendicular to the skin surface, *e.g.*, due to lift generated by the tag, the cup walls stretch increasing the internal volume and decreasing the internal pressure. Forces parallel to the skin surface (*e.g.*, drag) are resisted less effectively: a load applied to the stem of the cup (*i.e.*, a small distance away from the skin surface) will bend the stem and so increase the cup volume on the side away from the force. This generates a resisting force in combination with the friction of the cup lip against the skin surface. Because of these different attachment mechanisms, it is difficult to predict what the attachment force will be on the skin for a given combination of drag and lift forces.

To explore how fluid forces on the tag are transferred to the skin surface *via* the suction cups, we performed a pull test using an instrumented tag on a dead cetacean. The testing was conducted on a common dolphin (*Delphinus delphis*) cadaver that had been frozen shortly after death and thawed just prior to testing. A urethane positive of the Model A design was cast and four silicone suction cups were used to attach the model to the animal after the skin had been rinsed and wiped clean. Horizontal and vertical forces were applied to the tag using a cable, and force measurements were made with a load cell in the cable line (MLP-100; Transducer Techniques, Temecula, CA). The cable was fixed to the front of the body and aligned to the midline of the tag during horizontal loading, and was secured to the top of the tag in the center of the four cups for vertical loading. The loading was kept parallel to the cadaver for the horizontal tests, and perpendicular to the cadaver for the vertical tests. While efforts were made to maintain the horizontal and vertical alignment of the loading during the testing, the curvature of the cadaver and small alignment errors at the point of attachment with the cable likely prevented the application of a pure vertical or horizontal force. The tag was attached to three sites on the animal: (1) dorsally between the fin and the blowhole, (2) laterally above the flipper, and (3) laterally near the dorsal fin. Sites 1 and 3 are areas where tags are applied to free-swimming animals. Two trials were conducted at each site, and the applied forces covered the predicted range of forces for the Model A tag in 0–10 m/s flow. The corresponding vacuum force was calculated from pressure measurements collected using four pressure sensors (MPXV6115V p-xdrc; Freescale Semiconductor, Austin, TX) connected to the cups. Assuming that the vacuum holding the cup on to the skin is acting on a circular area (A_{skin}) with a diameter equal to that of the compressed cup lip (3 cm) then the attachment force of the system of four cups can be estimated from:

$$F_{\text{attachment}} = \sum_{i=1}^{4} \Delta P_i \bullet A_{\text{skin}}. \quad (2)$$

Results

All three models were tested using CFD simulations at flow rates of 0.25–10 m/s and at a range of orientations. Models A and B were then measured in the water tunnel at flows of 1–5.6 m/s to validate the CFD force estimates. Finally, pull-tests were performed on Model A to establish the skin loading corresponding to the flow forces on the tag.

Simulation Results

In 5.6 m/s inline flow, the Model A tag generated the smallest lift force (35 N), while the B design created the smallest drag force (4 N) of the designs (Table 2). In addition to the lowest drag force, the Model B design's drag coefficient, 0.09, was lower than both the Model A and C designs (0.40 and 0.13, respectively). Figures 4 and 5 illustrate the changes in the flow speed created by the A and B designs. Fluid flow was reduced in the proximity of both designs, with the speed loss being most evident for the Model A tag (Fig 4). Flow interference is also caused in the Model A design by the cup stems which create vortices that increase drag on the tag, while the screening around the Model B cups eliminated this disruption (Fig. 5). The Model C design was examined both with and without the foil and base sections. Simulations

Table 2. Simulated and measured drag and lift forces acting on the three tag designs in 5.6 m/s flow. The tags were oriented parallel to the flow.

	Simulated			Experimental		
Tag design	Lift (N)	Drag (N)	Coefficient of drag	Lift (N)	Drag (N)	Coefficient of drag
Model A	35	13	0.40	61	15	0.43
Model B	53	4	0.09	74	6	0.14
Model C	32	6	0.13	NA	NA	NA
Model C, no base	1	1	0.02	NA	NA	NA

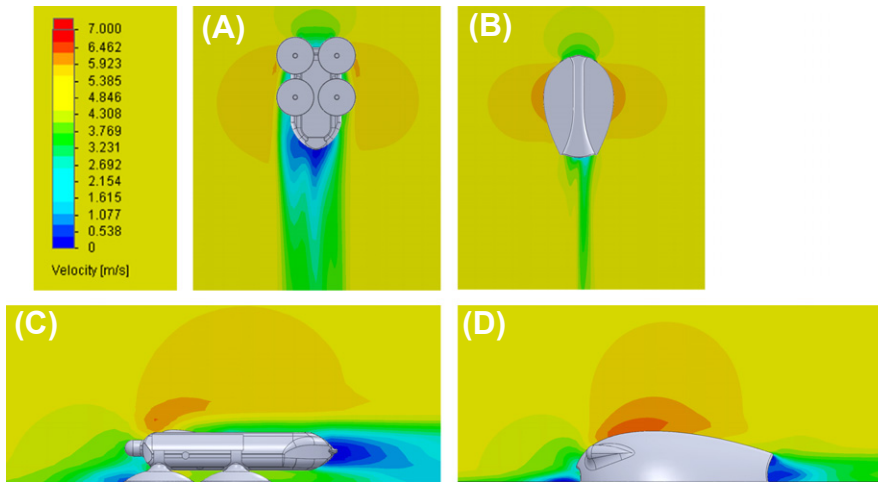

Figure 4. CFD simulation results for Models A (panels A and C) and B (panels B and D) in steady 5.6 m/s flow. The blue, yellow, and green regions are areas of reduced flow speed that generate forces on the tags. The upper panels show the flow speed over a horizontal cross-section at the tag midline. The lower panels show flow speed over a vertical cross-section at the centerline of the tag. The improved flow around Model B is evident in the smaller magnitude of blue coloration in the wake behind the tag.

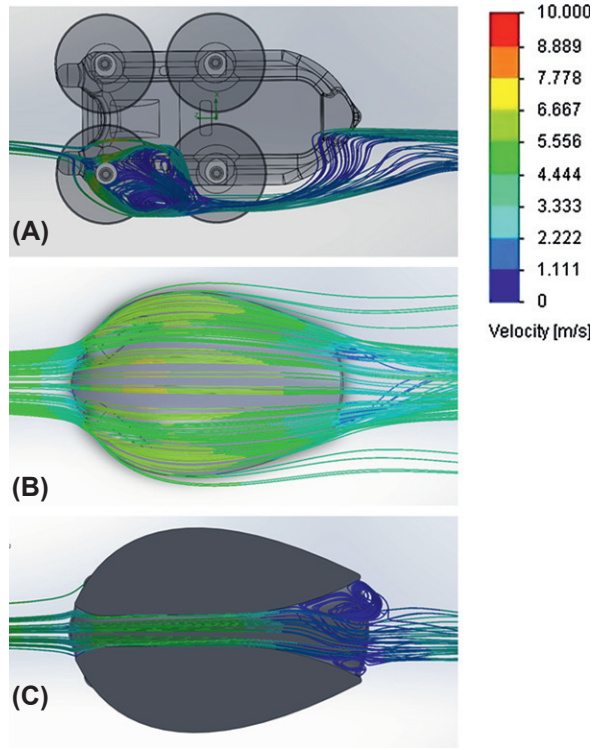

Figure 5. Detail of the flow path-lines around Models A and B. (A) Flow lines in the vicinity of a forward suction cup mounting pillar at a flow speed of 5.6 m/s demonstrating the flow disturbance created by the suction cups. The eddies and reduced speed result in larger forces acting on the tag. (B) Improved flow around the Model B tag design results from screening of the cups. (C) Flow through the channel underneath the Model B design showing flow detachment near the aft end of the channel.

of the Model C teardrop body alone showed a 83% reduction in the drag (1 N) and a 97% reduction in the lift (1 N) forces compared to the full Model C tag indicating that structure adjacent to the surface of the animal is the main source of lift.

The performance of the Model A and B designs was examined over a range of inline flow velocities (0.25–10 m/s; Fig. 6, 7). As expected, the drag, lift, and side forces for each design grew as the square of the flow speed over the range 0.25 m/s to 10 m/s, but the lateral forces were less than 2% of the largest force acting on the tag and so could be neglected. In 10 m/s inline flow the drag on the B design was 28 N smaller than the drag on the A design (41 N *vs.* 13 N; Fig. 6). However, the B design generated 53 N more lift than the A design (169 N *vs.* 116 N) at the same flow speed (Fig. 7). In simulation, lift was the dominant force on both tag designs at flow speeds above about 2 m/s.

Tags attached to free-swimming animals are seldom located perfectly in-line with the flow. The impact of tag orientation on the hydrodynamic forces is shown in Figures 8 and 9 for Models A and B, respectively. These simulation results were obtained at a constant flow (5.6 m/s) and with orientation from 0 to 180 degrees. Lift

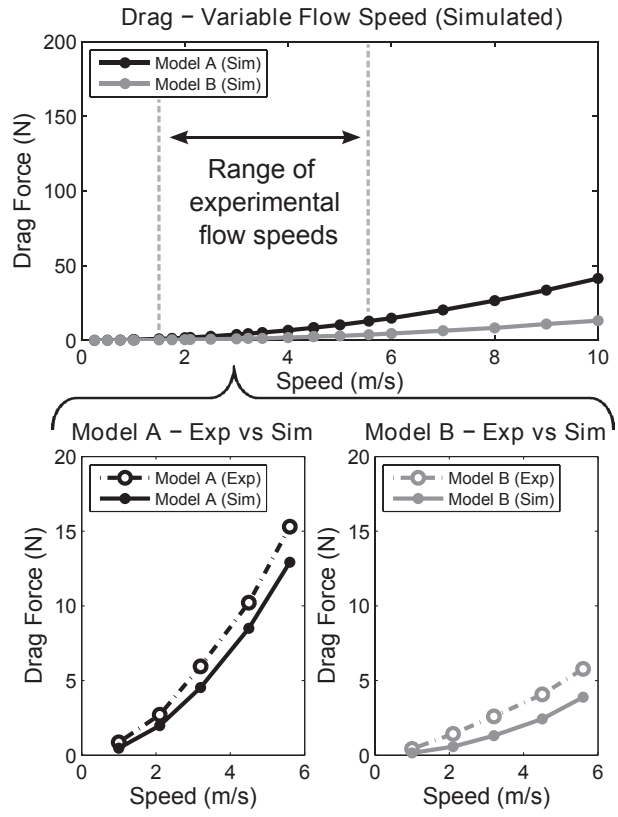

Figure 6. Simulation results for the drag forces acting on the Model A and B tags (top panel) in variable flow (0.25–10 m/s) with fixed orientation (0º). Measured results in variable flow speed (1–5.6 m/s) are compared to simulations for the Model A tag (bottom left panel) and Model B tag (bottom right panel).

was the dominant force component for both tags at all orientations with Model A producing consistently less lift than model B (Fig. 9, top panel). However, the drag of Model B was smaller than Model A at all orientations except 80° (Fig. 8, top panel). In both designs, the orientation of the tag with respect to the flow has a substantial impact on the total force. Total forces increased from 37 N and 53 N for Model A and B, respectively, at a 0º orientation, to a maximum total force of 71 N (Model A) and 90 N (Model B) at orientations near 130°.

Experimental Results: Model A vs. Model B

The water tunnel results confirm the relationships between force and flow rate (Fig. 6, 7, bottom panels) and orientation (Fig. 8, 9, bottom panels) established by simulation. Table 3 shows the root mean square error (RMS) differences between the experimentally measured and simulated forces acting on models A and B at five flow speeds and 0º orientation, and 12 orientations and 5.6 m/s flow. The experimental trials yielded consistently higher forces than predicted by simulation with the

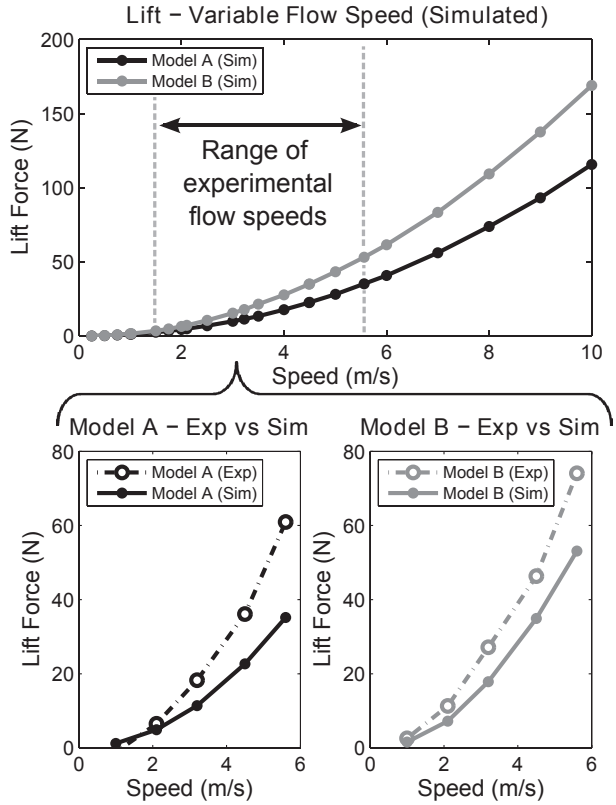

Figure 7. Simulation results for the lift forces acting on the Model A and B tags (top panel) in variable flow (0.25–10 m/s). Measured results in variable flow speed (1–5.6 m/s) are compared to simulations for the Model A tag (bottom left panel) and Model B tag (bottom right panel).

difference being most pronounced in lift (maximum of 19 N difference at 5.6 m/s). Nonetheless, the overall trends measured during the experimental trials agree well with the simulation results: the Model B tag generated less drag but larger lift than the Model A tag, and the forces on both tag designs increased in off axis flows (Fig. 6–9, bottom panels and Table 2).

Load Testing Results

The soft suction cups used on the tags had an average unloaded vacuum pressure of 10 kPa or 0.10 bar when first attached to the dolphin cadaver producing a total unloaded force on the skin surface of 31 N. Force was then applied along the length of the animal in the posterior direction to mimic drag on the tag. For longitudinal forces up to 15 N, pressure in the cups did not change and only the portion of the cups connected to the model body deformed under the load. As the force increased, the cup bodies began to deform resulting in a decrease in the internal cup pressure, *i.e.*, an increase in the cup attachment forces (Fig. 10, top panel). The average applied

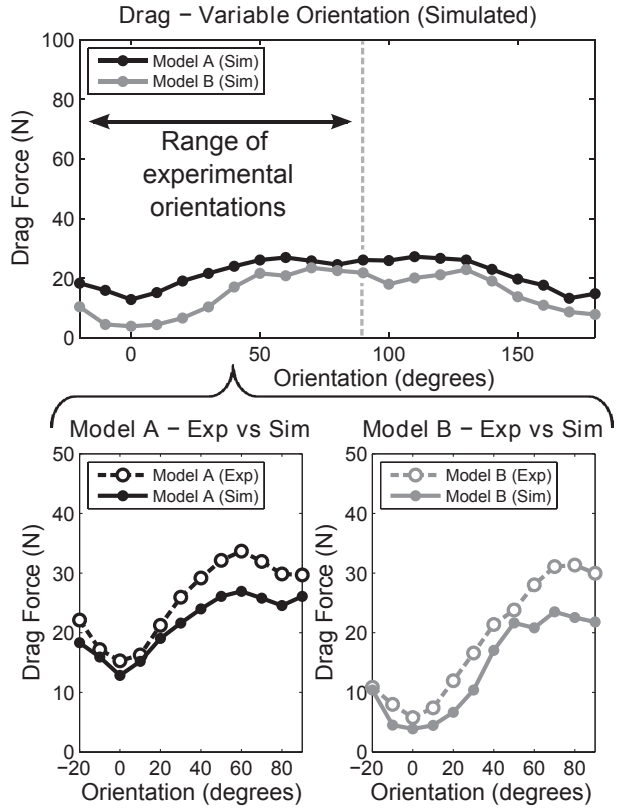

Figure 8. Simulation results for the drag forces acting on the Model A and B tags (top panel) in constant flow (5.6 m/s) as a function of orientation (–20º to 180º). Measured results as a function of orientation (–20º to 90º) in constant 5.6 m/s flow are compared to simulations for the Model A tag (bottom left panel) and Model B tag (bottom right panel).

force that resulted in sliding was comparable at sites 1 (75 N) and 2 (77 N) but lower at site 3 (64 N). These differences could be due to differing structure of the tissue layers at the three sites. All of these sliding forces are considerably larger than the drag force expected for Model A in 10 m/s flow (42 N). The corresponding average vacuum pressures in the cups at the onset of sliding were 24, 21, and 20 kPa for the three sites.

For forces applied perpendicular to the skin surface, *i.e.*, mimicking lift forces, the cups elongated in a direction parallel with the increasing force and a visible deformation of the skin surface was observed as skin was drawn into the cup by the increasing vacuum force. The average applied force at cup failure was 165 N at site 1, 147 N at site 2, and 181 N at site three (Fig. 10, lower panel). As for drag, all of these detachment forces are greater than the 115 N lift force predicted for Model A in 10 m/s flow. The average vacuum pressures just before cup failure were 50, 45, and 51 kPa at the three sites.

Both the simulated and water tunnel results indicate that lift forces are much larger than drag on the two models. Therefore, the total force transferred to the skin

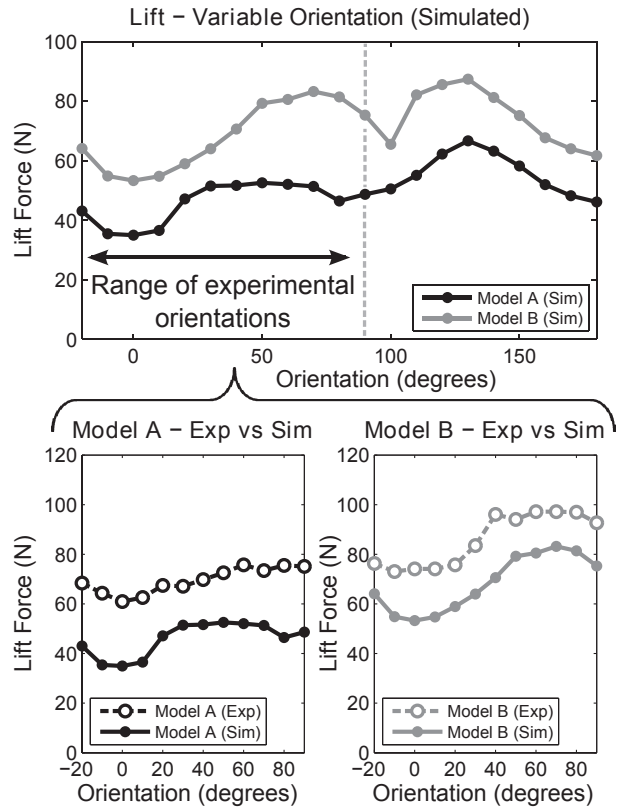

Figure 9. Simulation results for the lift forces acting on the Model A and B tags (top panel) in constant flow (5.6 m/s) as a function of orientation (–20° to 180°). Measured results as a function of orientation (–20° to 90°) in constant 5.6 m/s flow are compared to simulations for the Model A tag (bottom left panel) and Model B tag (bottom right panel).

Table 3. Root mean squared (RMS) errors in Newtons between the simulated and experimental results for the Model A and B tag designs. Squared errors are summed for (1) flow rates of 1–5.6 m/s in five steps with the tag oriented parallel to the flow (left hand two columns) and (2) for orientations of –20° to 90° in 10° steps in a constant 5.6 m/s flow (right hand columns).

	Variable flow RMS		Variable orientation RMS	
Force	Model A (N)	Model B (N)	Model A (N)	Model B (N)
Side	0.8	0.9	6.9	2.0
Drag	1.5	1.3	2.4	3.2
Lift	13.4	11.6	25.5	17.7
Overall	13.2	11.7	25.1	18.0

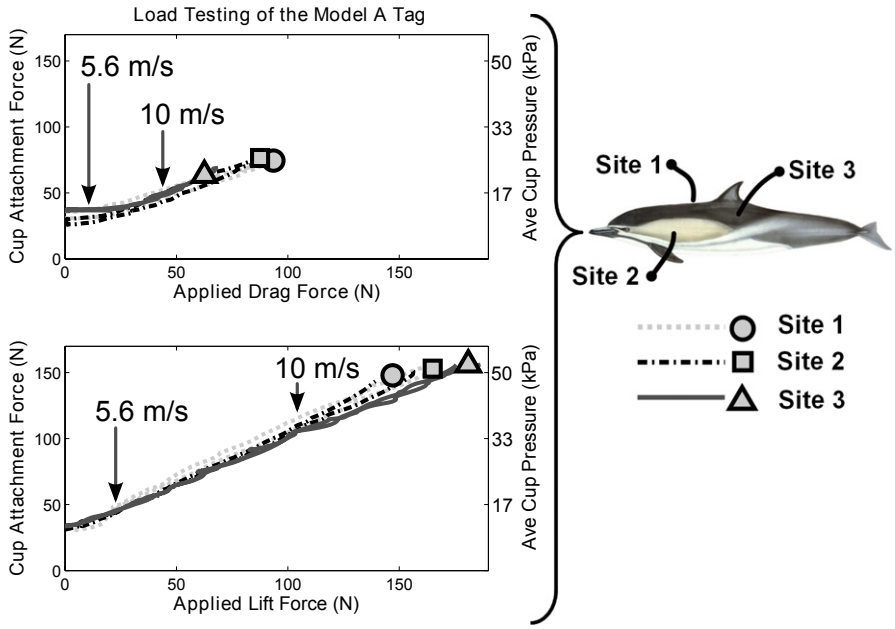

Figure 10. Experimental load testing of a Model A tag attached at three test sites on a common dolphin cadaver using four silicone suction cups. Applied force *vs.* calculated total cup attachment force at the four silicone suction cups are shown for lift (bottom panel) and drag (top panel) loading. The average pressure difference for the four cups is also shown on the right hand axis, where 1 atmosphere is approximately 100 kPa. Forces were applied *via* a line attached to the tag by pulling either perpendicular to the body (lift) or parallel (drag). The curves end where the cup attachment failed or the cups began to slide. The average of two trials at each site is shown in each panel.

surface can be estimated from the lift loading curves (Fig. 10, lower panel). These data have a regression line of

$$F_{\text{Trans}} = 0.72 \bullet F_{\text{Lift}} + 27N \tag{3}$$

with a 0.99 coefficient of determination (R^2). The model A and B tags aligned parallel to a flow of 5.6 m/s generate a lift of 61 and 74 N, respectively. Using Equation 3, the resulting total force on the skin will be about 71 and 80 N (or ~18 and ~20 N per cup), respectively. The corresponding vacuum pressures in the each cup will be approximately 25 and 28 kPa (0.25, 0.28 Bar).

Discussion

Hydrodynamic forces generated by fluid flow around a tag on an animal can have undesirable consequences: an increase in the animal's energy expenditure, creation of possible changes to swimming behavior, and stress at the attachment points between the tag and the animal that can cause discomfort and attachment failure. Our objective here is to improve the hydrodynamic housing design of a suction-cup

attached archival tag for the collection of acoustic and motion data, but our results are also applicable to other tag types. Following Pavlov *et al.* 2007, we used computer-aided design (CAD) and computational fluid dynamics (CFD) to estimate the forces generated by different housing designs over a range of flow conditions. Our results are broadly comparable with Pavlov *et al.* (2007) who predicted drag forces of 1–6.5 N for a fin-mounted tag for bottlenose dolphins (*Tursiops truncates*) with a maximum tag frontal area of 1,400 mm^2, over a fluid speed range of 0–8 m/s. In comparison, we predict drag forces of 1–14 N for tags with frontal areas of 2,200–3,800 mm^2, at fluid speeds of 0–10 m/s.

A critical step in applying CFD is the validation of simulation results with real measurements. This establishes the accuracy of the simulations and helps identify modeling assumptions that are not robust. Here we compared identical CAD models in simulations and, *via* 3D printed prototypes, in a water tunnel. The overall trends measured during the experimental trials agree well with the simulation results, but the drag and side forces were more accurately predicted than the lift forces (Table 3). This was particularly true for the drag and side forces in variable flow trials, where the RMS errors between simulation and experiment were in the range of 1 N over speeds from 1 to 5.6 m/s. In general, the measured forces were higher than the simulated forces suggesting that there are some force contributions that are not modeled effectively by CFD. One example is the surface texture of the 3D printed prototype, which will increase the measured drag but which is not practical to include in the CFD simulation because it would drastically increase the computational requirements. Other discrepancies could be due to the experimental setup in the water tunnel. In the experiment, the model was mounted on a 7.6 cm diameter disk that protruded slightly (1–3 mm) into the water tunnel, and was necessary to prevent the tag from contacting the grounding plate. The raised feature resulted in additional flow forces measured by the block gauges, but the disk protrusion was not included in the simulations. Further, the larger discrepancy between the simulated and experimental lift forces could be due to the water tunnel set up. While the grounding board surrounds the extension where the test piece is mounted to create a uniform ceiling for the test section, the space above the grounding board is flooded. As such, an artificial lifting force could be created because the flooded section above the extension arm has a constant pressure, while the lower portion of the plate experiences test section pressure. The exposed area of the extension below the grounding board will also add to the lift force. Based on prior experience and the close agreement of the simulated and experimental drag forces the actual lift force may be closer to the CFD results than the experimental results.

Tag Design Comparisons

Three tag designs were evaluated, each with advantages and disadvantages. The overall results demonstrate (1) that a smooth form (Model B) reduces drag, (2) that a small cross sectional area close to the attachment surface (Model A) reduces lift, and (3) the additional structure required to move a streamlined body away from the attachment surface (Model C) negates the benefit of the new position in the flow. The simulation results provide insight into the performance tradeoffs between a smooth form and a small cross-sectional area. Figure 4 shows a comparison of the flow speed around the Model A and B tags during inline 5.6 m/s flow. Reduced flow occurs both ahead of the tags (stagnation) and behind the tags (bluff body wake) with the speed loss most evident for the Model A tag. The smoother form of design B disrupts the

flow less and, in particular, greatly reduces the size of the wake. The streamlines near the cup stem and leading edge of the Model A cup are shown in more detail in Figure 5A. Vortices created by the circular cross section of the cup stems are evident between the cups, resulting in increased drag on the Model A tag. In contrast, the screening around the cups in the B design reduces the stagnant flow and shrinks the wake, resulting in drag reduction (Fig. 5B).

Lift forces arise from a pressure difference created by asymmetric flow above and below the tag. One approach to reduce lift is to minimize the width of the tag in the flow direction and therefore the footprint on the animal. However, this is not practical for a tag attached to an animal using suction cups, which require a large footprint on the skin surface. Narrow designs can be achieved by aligning the cups in a single row parallel to the flow. However, the resulting tags have high profiles that are vulnerable to detachment through contact with other animals, and lack the lateral stiffness in the attachment required for good acceleration data.

An alternative approach to reduce lift is to add features that direct the flow under the tag. This was the intention of the channel on the underside of Model B. However, this feature was not effective in reducing lift, and the bottom panel of Figure 5 illustrates why this might be so. The steady 5.6 m/s flow is slowed by the front of the tag to ~2.5 m/s at the channel entrance. As the fluid enters the channel, the velocity increases to ~4.5 m/s just before the smallest channel cross-section. Then, as the channel widens, the velocity of the fluid slows and becomes separated from the channel wall creating stagnant flow (0 m/s). In contrast, the velocity of the fluid passing over the top of the tag increases to ~7 m/s in areas, resulting in the lift-generating pressure differential. The simulations illustrate that the channel does direct and accelerate flow, but the detached flow in the channel cancels out the intended benefit. Future work to reduce lift should be directed at channel designs that eliminate flow separation and the introduction of housing features that redirect flow to counter lift (*e.g.*, spoilers).

In summary, the following design guidelines can be used to aid in the creation of hydrodynamic body-mounted tags:

(1) Minimize the frontal cross-sectional areas of the tag but maintain a smooth envelope to reduce drag.
(2) Cover exposed features, like the cups, to reduce stagnant flow and wake creation.
(3) Reduce lift by minimizing the attachment footprint and by adding features that reduce flow speed differences above and below the housing (*e.g.*, channels) or that redirect the flow to counter lift (*e.g.*, spoilers). If the tag orientation on the animal can vary, ensure that these added features will not increase forces at nonideal orientations.

Implications of the Results for Suction Cup Tag Attachments

The lift and drag forces generated by the tag must be resolved at the point of attachment if the tag is to remain on the animal. The four 45 mm diameter silicone suction cups used in all the tag designs are able to resist drag forces of 63–94 N and lift forces of 147–181 N depending on the attachment site (Fig. 10). Thus, the attachment is more than strong enough to resist predicted drag (42 N) and lift (115 N) forces on the A design at flows of up to 10 m/s. However, the increased lift of the B design may cause attachment failure at around 8 m/s, but the divergence of

the simulated and measured lift forces makes this rather uncertain. Cup detachment is likely to be a complex function of the loading and the substrate shape and properties, and so will not occur consistently at a predictable speed. Nonetheless, our results suggest that the suction cup attachment can withstand flow-induced loading at usual swimming speeds with only a nominal increase in vacuum pressure but failure may occur during bursts of speed or rapid maneuvers.

Drag loads of up to 20 N cause no significant deformation of the cup shape and therefore no change in the vacuum force at the skin surface. This implies that the unloaded vacuum force (approximately 30 N for the four cups at 10 kPa each) together with the friction between the cup and the skin surface is sufficient to oppose the expected drag forces at swimming speeds of up to 6 m/s for the A and B models. With drag forces larger than 20 N the cups work as dynamic anchors to oppose sliding tag motion with the elongated cup bodies generating larger vacuum forces in the cups. The loading that resulted in a sliding failure (63–94 N) was comparable at sites 1 and 2 but was lower at site 3, indicating that the texture of the skin surface or the material properties of the substrate may vary from site to site. Site 1 has significant subcutaneous fat, Site 2 overlies muscle inserting on the blade of the scapula, and Site 3 has increased blubber fiber content as part of the dorsal fin saddle. Surface roughness was not measured at the attachment sites but is uniformly low on dolphins. In contrast to drag loading, lift loading is countered directly by an increase in attachment force at the suction cups (Fig. 10). For the cups used, the unloaded attachment force was around ~7.5 N (10 kPa) per cup and increased to about 12 and 15 N (16 and 20 kPa) per cup for the A and B models in 5 m/s flow, respectively.

For a suction cup attachment, loads applied to the tag are translated into pressure loading on the skin. Suction cup attachments do not penetrate the skin, but the stress put on the skin, even at forces well below the failure force, could affect the skin. Gupta and Kumar used rigid walled cylinders and a 40 kPa pressure differential to create skin blistering in people (Gupta and Kumar 2000). The skin that formed the blister wall was harvested and transplanted to other areas of the subject's body. Time to blister formation was dependent on the diameter of the cylinder, magnitude of the pressure differential, anatomy of the tissue at the blister site, age of the subject, and temperature at the blister site. Interestingly, the application of too much pressure (66 kPa) resulted in bruising instead of blistering. All of these factors make it difficult to predict whether bruising will be created by a suction cup attachment on a marine mammal. However, the authors have observed visible discoloration and light swelling of the skin in captive animals that have carried a tag for periods ranging from 1 to 8 h using the relatively soft 45 mm diameter silicone suction cups described here. Although this observed tissue damage appeared to be relatively minor and reversible, it is a single anecdotal case and the impact of longer duration suction cup attachments on marine mammals requires further investigation. To address these issues, skin loading can be reduced by increasing cup diameter, using more cups with lower setup pressures, or a combination of the two. However, these solutions would require a larger footprint on the animal leading to increased lift forces and a diminishing return.

Conclusions

Computational fluid dynamics simulation provides a convenient and rapid environment in which to develop tag designs for marine animals. Here we show that the forces predicted by CFD simulation largely agree both in trend and magnitude with

those measured on models in a flow tank. This validation is a critical step for CFD to receive wide-spread use. Our simulation and experimental results confirm that drag forces on tags attached to the skin surface of marine animals can be significantly reduced by adopting a smooth hydrodynamic shape with a minimized frontal cross-sectional area, but that lift is the dominate force, particularly at swimming speeds above 5 m/s. The suction cups currently used to field tags are sufficient to resist lift and drag loading at swim speeds of up to 10 m/s depending on the tag design. Although strong lift forces cause direct detachment of the cups, the tag will tend to slide along the body at lower drag forces and this is likely to be the primary failure mode. The setup pressure differentials that create the attachment forces in the cups are low (10 kPa or 7.5 N per cup), but can increase five-fold under certain loading conditions. As such, the impact of the vacuum loading on the skin requires further evaluation.

Acknowledgments

This work was supported by NOPP with NSF funds through ONR Grant N00014-11-1-0113. The authors would also like to thank Tom Hurst, Enric Xargay, and Giovanni Fiore for helpful discussions, and Don Bunker and John Zseleczky of the United States Naval Academy Hydro Lab for their help with the water tunnel experiments. MJ was supported by NOPP and the MASTS pooling initiative (The Marine Alliance for Science and Technology for Scotland). MASTS is funded by the Scottish Funding Council (grant reference HR09011) and contributing institutions.

Literature Cited

Aguilar Soto, N., M. P. Johnson, P. T. Madsen, F. Díaz, I. Domínguez, A. Brito and P. Tyack. 2008. Cheetahs of the deep sea: Deep foraging sprints in short-finned pilot whales off Tenerife (Canary Islands). Journal of Animal Ecology 77:936–947.

Andrews, R. D., R. L. Pitman and L. T. Ballance. 2008. Satellite tracking reveals distinct movement patterns for type B and type C killer whales in the southern Ross Sea, Antarctica. Polar Biology 31:1461–1468.

Aoki, K., M. Amano, M. Yoshioka, K. Mori, D. Tokuda and N. Miyazaki. 2007. Diel diving behavior of sperm whales off Japan. Marine Ecological Press Series 349:277–287.

Cooke, S. J., S. G. Hinch, M. Wikelski, R. D. Andrews, L. J. Kuchel, T. G. Wolcott and P. J. Butler. 2004. Biotelemetry: A mechanistic approach to ecology. Trends in Ecology & Evolution 6:334–343.

Fish, F. E. 1998. Comparative kinematics and hydrodynamics of odontocete cetaceans: Morphological and ecological correlates with swimming performance. Journal of Experimental Biology 201:2867–2877.

Fish, F. E., and J. J. Rohr. 1999. Review of dolphin hydrodynamics and swimming performance. Technical Report 1801, SPAWAR Systems Center, San Diego, CA. 196 pp.

Fox, R. W., and A. T. McDonald. 1999. Introduction to fluid mechanics. Wiley, New York, NY.

Gupta, S., and B. Kumar. 2000. Suction blister induction time: 15 minutes or 150 minutes? Dermatologic Surgery 26:754–757.

Hanson, M. B. 2001. An evaluation of the relationship between small cetacean tag design and attachment durations: A bioengineering approach. Ph.D. dissertation, University of Washington, Seattle, WA. 221 pp.

Hooker, S. K., and R. W. Baird. 2001. Diving and ranging behaviour of odontocetes: A methodological review and critique. Mammal Review 31:81–105.

Johnson, M. P., and P. L. Tyack. 2003. A digital acoustic recording tag for measuring the response of wild marine mammals to sound. IEEE Oceanic Engineering Society 28:3–12.
Madsen, P. T., R. Payne, N. U. Kristiansen, M. Wahlberg, I. Kerr and B. Møhl. 2002. Sperm whale sound production studied with ultrasound time/depth-recording tags. The Journal of Experimental Biology 205:1899–1906.
Mate, B., R. Mesecar and B. Lagerquist. 2007. The evolution of satellite-monitored radio tags for large whales: One laboratory's experience. Deep Sea Research Part II: Topical Studies in Oceanography 54:224–247.
Miller, P. J. O., M. P. Johnson and P. L. Tyack. 2004. Sperm whale behaviour indicates the use of echolocation click buzzes 'creaks' in prey capture. Proceedings of the Royal Society B-Biological Sciences 271:2239–2247.
Munson, B. R., D. F. Young and T. H. Okiishi. 2006. Fundamentals of fluid mechanics. 5th edition. John Wiley & Sons, Inc., Hoboken, NJ.
Pavlov, V. V., R. P. Wilson and K. Lucke. 2007. A new approach to tag design in dolphin telemetry: Computer simulations to minimize deleterious effects. Deep Sea Research Part II: Topical Studies in Oceanography 54:404–414.
Pavlov, V. V., and A. M. Rashad. 2011. A non-invasive dolphin telemetry tag: Computer design and numerical flow simulation. Marine Mammal Science 28:E16–E27.
Read, A. J., and A. J. Westgate. 1997. Monitoring the movements of harbour porpoises (*Phocoena phocoena*) with satellite telemetry. Marine Biology 130:315–322.
Ropert-Coudert, Y., and R. P. Wilson. 2005. Trends and perspectives in animal-attached remote sensing. Frontiers in Ecology and the Environment 3:437–444.
Ropert-Coudert, Y., R. P. Wilson, K. Yoda and A. Kato. 2007. Assessing performance constraints in penguins with externally-attached devices. Marine Ecology Progress Series 333:281–289.
Sato, K., Y. Watanuki, A. Takahashi, P. J. O. Miller, *et al*. 2007. Stroke frequency, but not swimming speed, is related to body size in free-ranging seabirds, pinnipeds and cetaceans. Proceedings of the Royal Society B-Biological Sciences 274:471–477.
Schultz, M. P., and K. A. Flack. 2003. Turbulent boundary layers over surfaces smoothed by sanding. Journal of Fluid Engineering 125:863–870.
van Dam, R. P., P. J. Ponganis, K. V. Ponganis, D. H. Levenson and G. Marshall. 2002. Stroke frequencies of emperor penguins diving under sea ice. Journal of Experimental Biology 205:3769–3774.
Viviant, M., A. W. Trites, D. A. S. Rosen, P. Monestiez and C. Guinet. 2010. Prey capture attempts can be detected in Steller sea lions and other marine predators using accelerometers. Polar Biology 33:713–719.
Watanabe, Y. Y., K. Sato, Y. Watanuki, *et al*. 2011. Scaling of swim speed in breath-hold divers. Journal of Animal Ecology 80:57–68.
Weber, P. W., L. E. Howle, M. M. Murray and F. E. Fish. 2009. Lift and drag performance of odontocete cetacean flippers. Journal of Experimental Biology 212:2149–2158.
Weber, P. W., L. E. Howle and M. M. Murray. 2011. Computational evaluation of the performance of lifting surfaces with leading-edge protuberances. Journal of Aircraft 77:591–600.
Wilson, R. P., and C. R. McMahon. 2006. Measuring devices on wild animals: What constitutes acceptable practice? Frontiers in Ecology and the Environment 4:147–154.
Wilson, R. P., W. S. Grant and D. C. Duffy. 1986. Recording devices on free-ranging marine animals: Does measurement affect foraging performance? Ecology 67:1091–1093.
Wilson, R. P., J. M. Kreye, K. Lucke and H. Urquhart. 2004. Antennae on transmitters on penguins: Balancing energy budgets on the high wire. Journal of Experimental Biology 207:2649–2662.

Received: 4 February 2013
Accepted: 12 August 2013